

# Modelling the Spoon IRS diagnostic diagram

Michael Rowan-Robinson<sup>1</sup>\* and Andreas Efsthathiou<sup>2</sup>

<sup>1</sup>*Astrophysics Group, Blackett Laboratory, Imperial College of Science Technology and Medicine, Prince Consort Road, London SW7 2AZ*

<sup>2</sup>*School of Sciences, European University Cyprus, Diogenes St, Engomi, 1516 Nicosia, Cyprus*

Accepted 2009 June 29. Received 2009 May 29; in original form 2009 March 16

## ABSTRACT

We explore whether our models for starbursts, quiescent star-forming galaxies and for active galactic nuclei (AGN) dust tori are able to model the full range of Spitzer Infrared Spectrograph (IRS) spectra measured with *Spitzer*. The diagnostic plot of 9.7  $\mu\text{m}$  silicate optical depth versus 6.2  $\mu\text{m}$  polycyclic aromatic hydrocarbon (PAH) equivalent width, introduced by Spoon and coworkers in 2007, gives a good indication of the age and optical depth of a starburst, and of the contribution of an AGN dust torus. However, there is aliasing between age and optical depth at later times in the evolution of a starburst, and between age and the presence of an AGN dust torus. Modelling the full IRS spectra and using broad-band 25–850  $\mu\text{m}$  fluxes can help to resolve these aliases. The observed spectral energy distributions require starbursts of a range of ages with initial dust optical depth ranging from 50–200, optically thin dust emission (‘cirrus’) illuminated by a range of surface brightnesses of the interstellar radiation field, and AGN dust tori with a range of viewing angles.

**Key words:** star: formation – galaxies: evolution – infrared: galaxies – galaxies: starburst – cosmology: observations.

## 1 INTRODUCTION

The wealth of mid- and far-infrared (far-IR) spectroscopy of galaxies from *Infrared Space Observatory (ISO)* and *Spitzer* have provided a challenge for models of their spectral energy distributions (SEDs), which has been tackled by several groups. Over the past 20 yr, we have developed increasingly sophisticated radiative transfer models for different types of IR galaxy, for example, for starburst galaxies (Rowan-Robinson & Crawford 1989; Rowan-Robinson & Efsthathiou 1993; Efsthathiou, Rowan-Robinson & Siebenmorgen 2000, hereafter ERRS00), active galactic nuclei (AGN) dust tori (Rowan-Robinson & Crawford 1989; Efsthathiou & Rowan-Robinson 1995; Rowan-Robinson 1995) and quiescent (‘cirrus’) galaxies (Rowan-Robinson 1992; Efsthathiou & Rowan-Robinson 2003, hereafter ERR03; Efsthathiou & Siebenmorgen 2009). Each of these model types involves at least two significant model parameters, so there is a great wealth of possible models, particularly as a galaxy SED may be a mixture of all three types. Starburst models have also been developed by Silva et al. (1998), Takagi, Arimoto & Hanami (2003), Dopita et al. (2005) and Siebenmorgen & Krügel (2007). Other works on radiative transfer modelling of the torus in AGN have been presented by Pier & Krolik (1992), Granato & Danese (1994), Nenkova, Ivezić & Elitzur (2002), Nenkova et al. (2008), Dullemond & van Bemmelen (2005), Hönig et al. (2006) and Schartmann et al. (2008). Other works on radiative transfer mod-

elling of cirrus galaxies have been presented by Silva et al. (1998), Dale et al. (2001) and Piován, Tantaló & Chiosi (2006).

Often, however, we have only limited broad-band data available and in this situation it is more illuminating to use a small number of IR templates to match the observed IR colours (e.g. Rowan-Robinson & Crawford 1989; Rowan-Robinson 1992, 2001; Rowan-Robinson & Efsthathiou 1993, Rowan-Robinson et al. 2004, 2005, 2008). These templates have proved remarkably successful in matching observed Spitzer SEDs, including cases where IRS data are available (Rowan-Robinson et al. 2006; Farrah et al. 2008; Hernán-Caballero et al. 2009).

Spoon et al. (2007) have published a very interesting diagnostic diagram for starburst and active galaxies, which plots the strength of the silicate 9.7  $\mu\text{m}$  feature against the equivalent width (EW) of the 6.2  $\mu\text{m}$  polycyclic aromatic hydrocarbon (PAH) feature for 180 galaxies with Spitzer IRS spectra. In this paper, we explore how well our models fit the distribution of galaxies in this diagram.

## 2 DESCRIPTION OF THE MODELS

### 2.1 AGN torus models

The most important constraint on early models for the torus in AGN (Pier & Krolik 1992; Granato & Danese 1994; Efsthathiou & Rowan-Robinson 1995) was provided by mid-IR spectroscopic observations from the ground in the 8–13  $\mu\text{m}$  window by (Roche et al. 1991). The observations showed moderate absorption features in type 2 AGN and featureless spectra in type 1 AGN. By comparison, the flared

\*E-mail: mrr@imperial.ac.uk

discs (whose thickness increases linearly with distance from the central source) of Efstathiou & Rowan-Robinson (1990, Efstathiou & Rowan-Robinson 1995) and Granato & Danese (1994) showed strong silicate emission features when observed face-on. The cylindrical geometry and high optical depth of the Pier & Krolik models eliminated the emission features but the overall spectra were rather narrow. Granato & Danese suggested that the silicate grains are destroyed by shocks in the inner part of the torus. Efstathiou & Rowan-Robinson proposed that tapered discs (whose thickness increases with distance from the central source in the inner part of the disc but tapers off to a constant value in the outer disc) with a density distribution that followed  $r^{-1}$  could give flat spectra in the mid-IR for an opening angle of around  $45^\circ$  and an equatorial optical depth of 1000 at  $1000 \text{ \AA}$ . Models with a smaller opening angle predicted face-on spectra with shallow silicate absorption features whereas models with a larger opening angle showed weak emission features. Recent *Spitzer* observations showed weak emission features in quasars and weak absorption features in Seyfert 1 galaxies (e.g. Hao et al. 2005, 2007; Siebenmorgen et al. 2005; Spoon et al. 2007). The tapered discs of Efstathiou & Rowan-Robinson, in combination with the starburst models of ERRS00, which are described below, have been very successful in fitting the SEDs of a number of AGN (e.g. Alexander et al. 1999; Ruiz et al. 2001; Farrah et al. 2003; Efstathiou & Siebenmorgen 2005). More recently, there has been interest in clumpy torus models (Nenkova et al. 2002, 2008; Dullemond & van Bemmelen 2005; Hönl et al. 2006), which as suggested by Rowan-Robinson (1995) also display weaker silicate features.

In this paper, we will use the tapered disc models of Efstathiou & Rowan-Robinson (1995). The models assume that the dust is smoothly distributed in the disc. However, this distribution may be considered a reasonable approximation to a clumpy dust distribution if the mean distance between clouds is comparable to their size. For this paper, we have explored a model in which we fix the equatorial  $1000 \text{ \AA}$  optical depth at 1000, the opening angle of the torus at  $60^\circ$  and the ratio of inner to outer cloud radii ( $r_i/r_o$ ) at 0.01. The opening angle as discussed above controls the behaviour of the silicate feature in the face-on case. The ratio of inner to outer disc radii controls the width of the SED but also the silicate feature strength because, for the same equatorial optical depth, a more extended disc is more optically thin in lines of sight perpendicular to the plane of the disc than a more compact disc. The reason for choosing this particular model is that it gives the strongest silicate emission feature when the torus is viewed face-on and can, therefore, match the silicate strength of the quasars in the sample. The SED of the torus is computed for 74 inclinations which are equally spaced in the interval 0 to  $90^\circ$ .

## 2.2 Starburst models

ERRS00 developed a starburst model that has three main features. The first feature of the model is that it incorporates the stellar population synthesis model of Bruzual & Charlot (1993) that gives the spectrum of the stars as a function of their age. We use the table that assumes a Salpeter Initial Mass Function (IMF) and stellar masses in the range  $0.1\text{--}125M_\odot$ . The second important feature of the model is that we carry out detailed radiative transfer that takes into account multiple scattering from grains and incorporates a dust model that includes small transiently heated grains and PAH molecules as well as large classical grains. The calculation of the emission of the small grains and PAHs is according to the method of Siebenmorgen & Krügel (1992). The third feature of the model

is that it incorporates a simple model for the evolution of the giant molecular clouds that constitute the starburst once a stellar cluster forms instantaneously at the centre of the cloud. The most important characteristic of this evolutionary scheme is that by about 10 Myr after star formation, the expansion of the H II region leads to the formation of a cold narrow shell of gas and dust. This naturally explains why the mid-IR spectra of starburst galaxies are dominated by the PAH emission and not by the emission of hot dust. The predicted spectra of the molecular clouds, therefore, shift to longer wavelengths with age and show stronger PAH EWs. Another effect of ageing is that the clouds get more optically thin and, therefore, the silicate features get shallower. The sequence of molecular clouds at different ages can be convolved with a star formation history to give the spectrum of a starburst at different ages.

ERRS00 showed that the *IRAS* colours of starburst galaxies can be modelled with starbursts whose star formation rate decays exponentially with an e-folding time  $\tau$  of 20 Myr. The choice of the other model parameters assumed by ERRS00 (average density  $n_{av}$ , star formation efficiency  $\eta$  and giant molecular cloud mass  $M_{GMC}$ .) was discussed by ERRS00 (Section 3) and was found to be in agreement with other indicators for the starburst galaxy M82. This choice of parameters gave rise to an initial optical depth of the molecular clouds in the *V* band  $\tau_V$  of 50. Rowan-Robinson & Efstathiou (1993) showed that the ultraluminous IR galaxies such as Arp220 are up to a factor of four more optically thick than starbursts like M82 and NGC 1068. Rather than computing a four-parameter grid of models, which would be impractical, we fixed  $\tau$  at 20 Myr and varied  $n_{av}$ ,  $\eta$  and  $M_{GMC}$  to give four discrete values of  $\tau_V$  (50, 100, 150 and 200) that span the range suggested by observations. In other words, we treat  $\tau_V$  as an effective free parameter of the model. The spectra are computed for 11 different ages ranging from 0 to 72 Myr. This sequence of models, in combination with the AGN torus models discussed above, has been shown by Farrah et al. (2003) to be in good agreement with the SEDs of 41 ultraluminous IR galaxies.

## 2.3 Cirrus models

ERR03 presented an extension of the ERRS00 model that allowed the calculation of cirrus models as well as a combination of starburst and cirrus. This model is much simpler than the ‘GRASIL’ model developed by Silva et al. (1998) or the model of Piovan et al. (2006) but as it has been shown by ERR03 the calculated spectra are in good agreement with the SEDs of local galaxies dominated by cirrus. The first step in this model involves the specification of the spectrum of starlight for which we have two options. We either use the Bruzual & Charlot table and an assumed star formation history or we use the spectrum of the interstellar radiation field (ISRF) in the solar neighbourhood Mathis, Mezger & Panagia (1983). In the first option, we assume (as in the case of the starburst model) that the star formation rate declines exponentially with an e-folding time  $\tau$ . For the emission of stars that formed in the last  $t_m$  years, we use the spectrum computed by the `STARBURST` code. We then scale the spectrum of starlight by varying the parameter  $\psi$  which is the ratio of the bolometric intensity of starlight to the bolometric intensity of the local interstellar radiation field (ISRF). Finally, we illuminate the dust with the starlight and calculate its IR spectrum. The code also provides the option to attenuate the starlight, by assuming a visual extinction  $A_V$  and calculate the spectrum from the UV to the millimeter by self-consistently reprocessing the energy absorbed in the optical/UV to the IR.

### 3 THE SPOON DIAGRAM

We now test whether our suite of models, tuned to fit the broad-band SEDs from 1  $\mu\text{m}$  to 1 mm, can explain the distribution of galaxies in the diagnostic diagram developed by Spoon et al. (2007), strength of 9.7  $\mu\text{m}$  silicate feature versus EW of 6.2  $\mu\text{m}$  PAH feature. A difficulty in defining the strengths of features in the mid-IR is defining the underlying continuum. The spectra are almost always very strongly modified both by the broad PAH emission features and by the broad silicate (generally absorption) features. Spoon et al. (2007) used several approaches to define the continuum, usually employing spline fits to the emission at three selected wavelengths. The resulting continua are plausible but somewhat arbitrary. Here, we adopt a more uniform approach, although it is no less vulnerable to contributions from unaccounted for absorption or emission features. In the region of the 6.2  $\mu\text{m}$  feature, we use a log–log interpolation between 5.85 and 6.6  $\mu\text{m}$  and in the region of the 9.7  $\mu\text{m}$  feature we use log–log interpolation between 8.2 and 12.0  $\mu\text{m}$ , to define the underlying continuum. We are, therefore, assuming that the latter has a power-law form between these selected end points.

Fig. 1 shows the Spoon diagram for a selection of our starburst models (ERRS00), compared with the Spoon et al. (2007) data for 180 starburst galaxies or AGN, showing the variation of just two model parameters, the age of the starburst, and the initial optical depth to the centre of a GMC.

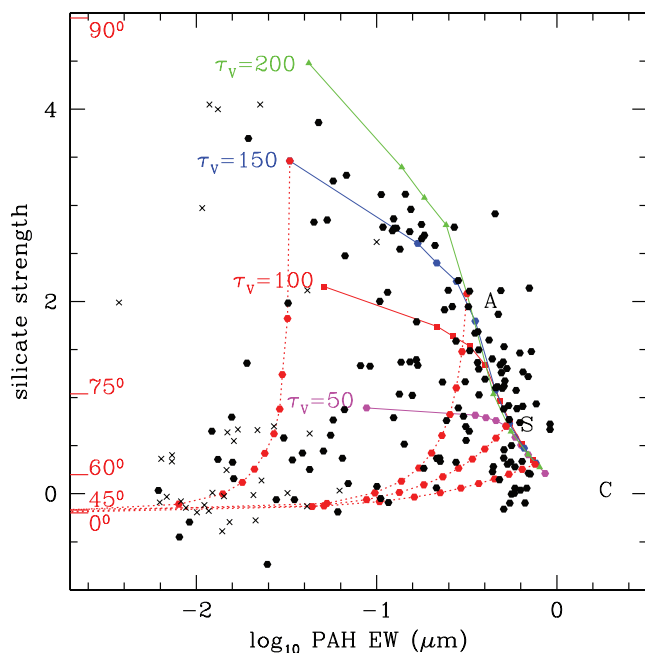


**Figure 1.** The Spoon diagram (Spoon et al. 2007): optical depth of 9.7  $\mu\text{m}$  silicate feature versus EW of 6.2  $\mu\text{m}$  PAH feature. Black filled circles are data points from Spoon et al. (2007), crosses denote upper limits to 6.2  $\mu\text{m}$  EW. Green, blue, red and magenta solid curves are sequences of starburst models with ages 0 (top) 6.6–10–16–26–37–45–56–72 (bottom) Myr and  $A_V = 200, 150, 100$  and 50, respectively, from Efstathiou et al. (2000). Labels A, S and C denote ‘Arp 220’, and ‘M82’ starbursts, and ‘cirrus’ (quiescent) galaxy templates used by Rowan-Robinson (2000). Red dotted curves are mixture lines between a face-on AGN dust torus and four starbursts with  $(t(\text{Myr}), A_V) = (0, 150), (26, 200), (26, 50)$  and  $(72, 50)$ . Red bars on the left axis denote the 9.7  $\mu\text{m}$  silicate optical depth for AGN dust torus model (opening angle 60°) viewed from inclinations 0, 45, 60, 75, 90°.

For AGN dust tori, we indicate in Fig. 1 the range of 9.7  $\mu\text{m}$  feature strengths as a function of viewing angle for one of these AGN dust torus models, a tapered disc with opening angle 60° (see above for other parameters). The 6.2  $\mu\text{m}$  EW is zero for these dust torus models, since we assume that in AGN environments the intensity of UV radiation is too high for the survival of very small grains or large molecules.

Mixture lines are shown between a type 1 AGN dust torus (face-on viewing) and two of our starburst models, those which have been used by Rowan-Robinson (2001) and Rowan-Robinson et al. (2005, 2008) to approximate to an M82 starburst and an Arp 220 (higher optical depth) starburst, to a young starburst ( $t = 0, A_V = 150$ ) and to an old starburst ( $t = 72 \text{ Myr}, A_V = 50$ ).

The models bracket the observed distribution remarkably well. Young starbursts are well differentiated by the 9.7  $\mu\text{m}$  feature strength for different  $A_V$  but at later times the sequences for different  $A_V$  converge, i.e. there is aliasing between starburst age and the optical depth. There is also aliasing between starbursts of young age and mixtures between AGN dust tori and older starbursts. This diagram on its own is not capable of resolving these aliases. The full IRS spectrum does offer a stronger handle on model parameters, especially when combined with photometry at longer wavelengths.

To illustrate the latter, we also show, in Fig. 2, the 100–60–25 (left-hand panel) and 850–100–60 (right-hand panel)  $\mu\text{m}$  colour–colour diagrams, for our starburst model sequences and for a series of cirrus models in which optically thin dust is illuminated by light with the spectrum of the local ISRF, with intensity  $\psi = 1, 2, 5, 10$ , where  $\psi$  denotes the ratio of the intensity of the radiation field to that in the solar neighbourhood. The 100–60–25  $\mu\text{m}$  data are from the Imperial IRAS FSC redshift (IIFSCz) catalogue of Wang & Rowan-Robinson (2009), with the restriction  $z < 0.3$ . The 850–100–60  $\mu\text{m}$  data are from Dunne et al. (2000), Rigopoulou, Lawrence & Rowan-Robinson (1996), Fox (2002), Clements et al (2009) and from a literature compilation by Chaniai (in preparation), with the restriction that  $z < 0.2$ . The 100–60–25  $\mu\text{m}$  diagram is sensitive to both the age of the starburst and the optical depth. Objects with higher values of S100/S60 require a quiescent (‘cirrus’) contribution. A complication of these far-IR colour–colour diagrams as diagnostics is the effect of redshift and there is a strong benefit in using rest-frame features as in Fig. 1.

While the main ridge of objects in the Spoon diagram (Fig. 1) could be modelled as a single sequence of starbursts of different ages, with  $A_V \sim 150$ . It is clear from the 100–60–25  $\mu\text{m}$  diagram (Fig. 2, left-hand panel) that the full range of  $A_V$  from 50 to 200 is needed. The broad-band colour–colour diagrams (Figs 2, left- and right-hand panel) both require that the starbursts models be mixed with an optically thin ‘cirrus’ contribution, with  $\psi$  in the range 2–10. Some of the outliers in the 850–100–60  $\mu\text{m}$  colour–colour diagram (Fig. 2, right-hand panel) may be due to inaccurate 850  $\mu\text{m}$  integrated fluxes, but there is a hint that some galaxies may contain more cold dust than predicted in these models. Finally, both the Spoon diagram, the 100–60–25  $\mu\text{m}$  diagram (Fig. 2, left-hand panel), and individual SEDs demonstrate the need in many cases for an additional component due to an AGN dust torus. Thus, the broad set of components (starbursts, cirrus, AGN dust torus) originally introduced by Rowan-Robinson & Crawford (1989) to account for the IRAS 12–100  $\mu\text{m}$  colours still hold, and encompass what we see in IR galaxy SEDs, albeit with considerable refinement.

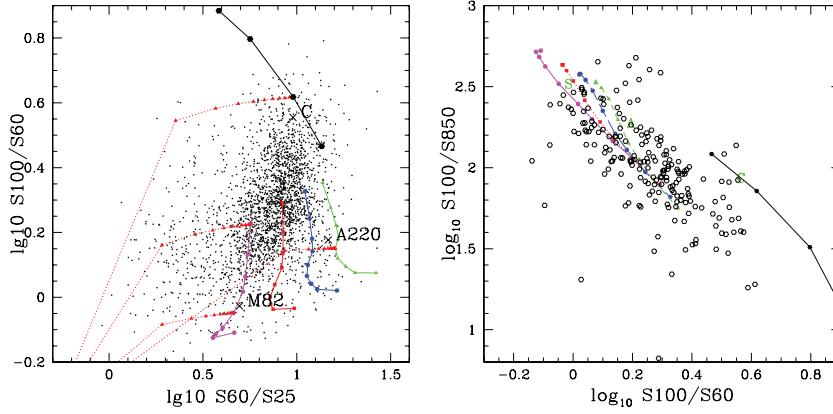


**Figure 2.** Far IR colour–colour diagrams. Left-hand panel: 100–60–25  $\mu\text{m}$ , data from IIFSCz catalogue (Wang & Rowan-Robinson 2009). RH 850–100–60  $\mu\text{m}$ , data from literature compilation by Chaniai (in preparation). Starburst and AGN dust torus mixture models as in Fig. 1. Youngest starburst models have lowest values of  $S(100)/S(60)$ . Black filled circles and solid curve: sequence of cirrus models with  $\psi = 1, 2, 5, 10$  (lowest value of  $S(100)/S(60)$ ).

#### 4 DETAILED FITS TO SEDS OF AVERAGE SPECTRAL CLASSES FROM SPOON ET AL. (2007)

Spoon et al. (2007) divide their diagnostic diagram into eight regions and generate a mean IRS spectrum for the galaxies in each region. In Figs 3–6, we show some of our model fits for these mean IRS spectra. Note that our models do not incorporate the 12.8  $\mu\text{m}$  Neii

line. Fits could probably be improved with a finer grid of models. In Fig. 5 (right-hand panel), we have included a cirrus model to show how similar this is to an old starburst at 5–40  $\mu\text{m}$ .

Such average SEDs give us some idea of the minimal set of templates needed to characterize IR galaxy spectra. But because of the strong evolution of individual SEDs as a starburst ages and the possible aliasing between starburst age, initial optical depth and possible presence of an AGN dust torus, galaxies at very different

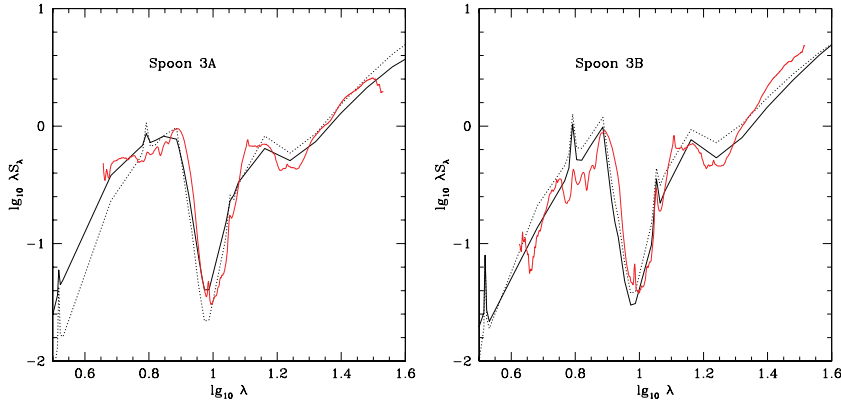


**Figure 3.** Left-hand panel: SED fits to Spoon et al. (2007) mean spectral class 3A. Solid curve: starburst  $t = 0$  Myr,  $A_V = 100$ , dotted curve: starburst  $t = 6.6$ ,  $A_V = 150$ . Right-hand panel: mean spectral class 3B. Solid curve: starburst  $t = 26$  Myr,  $A_V = 200$ , dotted curve: starburst  $t = 16$ ,  $A_V = 150$ .

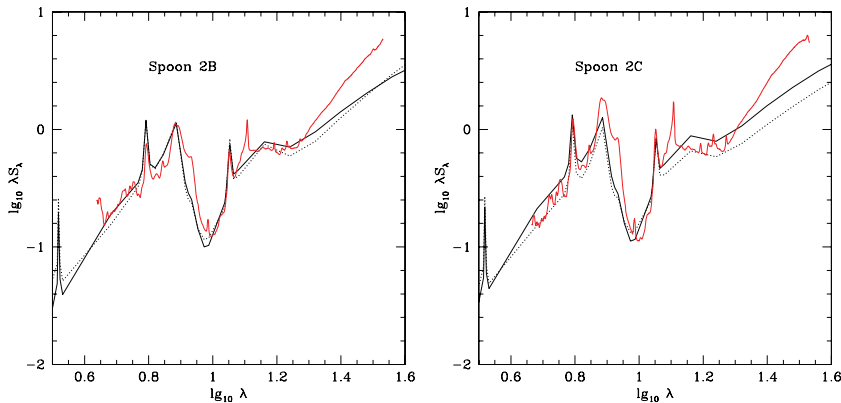


**Figure 4.** Left-hand panel: SED fits to Spoon et al. (2006) mean spectral class 2B. Solid curve: starburst  $t = 26$  Myr,  $A_V = 100$ , dotted curve: starburst  $t = 37$  Myr,  $A_V = 150$ . Right-hand panel: mean spectral class 2C. Solid curve: starburst  $t = 26$  Myr,  $A_V = 100$ , dotted curve: starburst  $t = 37$  Myr,  $A_V = 100$ .

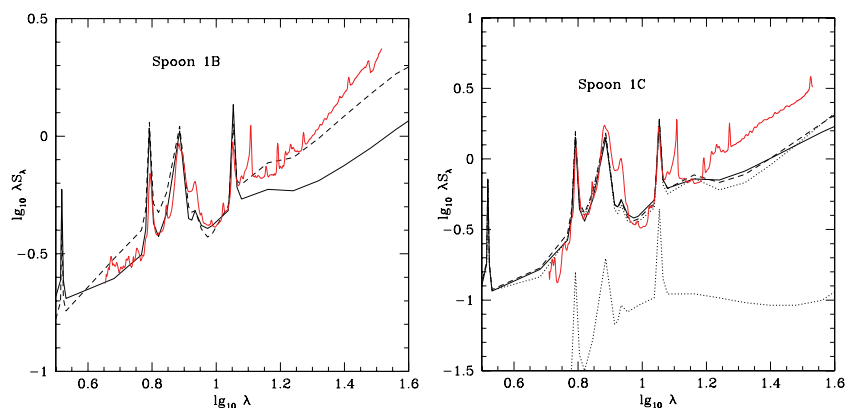


**Figure 5.** Right-hand panel: SED fits to Spoon et al. (2006) mean spectral classes 1B. Solid curve: mixture of starburst  $t = 72$  Myr,  $A_V = 50$  and face-on AGN dust torus, broken curve: mixture of starburst  $t = 26$  Myr,  $A_V = 50$  and face-on AGN dust torus. Right-hand panel: mean spectral class 1C. Solid curve: starburst  $t = 72$  Myr,  $A_V = 50$ , broken curve: starburst  $t = 72$  Myr,  $A_V = 100$ , dotted curve: starburst  $t = 72$  Myr,  $A_V = 150$ . Displaced dotted curve: cirrus model with  $\psi = 5$ .

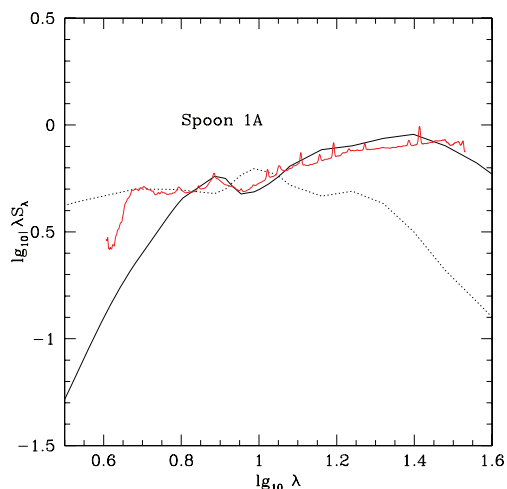


**Figure 6.** SED fits to Spoon et al. (2006) mean spectral classes 1A. Solid curve: AGN dust torus, inclination  $77^\circ$ . Dotted curve: AGN dust torus, face-on.

stages of their evolution may be being combined together in these averages. The 1A average spectrum (Fig. 6) certainly looks like an average together of AGN dust tori viewed at very different inclinations. In future work, we plan to model a substantial sample of individual galaxy SEDs where IRS data are available.

## 5 DISCUSSION AND CONCLUSIONS

Our models for starbursts, quiescent star-forming galaxies and for AGN dust tori are able to model the full range of IRS spectra measured with *Spitzer*. The Spoon et al. (2007) diagnostic diagram gives a good indication of the age and optical depth of a starburst, and of the contribution of an AGN dust torus. There are good possibilities of determining the age of a starburst from its spectrum and this has important implications for understanding the evolution of starburst and quasar activity in galaxies. However there is aliasing between age and optical depth at later times in the evolution of a starburst, and between age and the presence of an AGN dust torus.

The use of a small number of templates to model far-IR and sub-millimetre SEDs (Rowan-Robinson 2001) has obvious limitations, given the large number of potential model parameters. A significant

improvement to future analyses of this type might be to add an additional template corresponding to a young starburst, as in the mixture lines shown in Fig. 1. Although these represent a small fraction of the IR galaxy population ( $<10$  per cent), they are of great interest for evolutionary studies. An old starburst, which might also be desirable to bracket the full range of observed starburst, differs only slightly from a quiescent (cirrus) galaxy, at least in the mid-IR (see Fig. 5).

## ACKNOWLEDGMENTS

We thank Henrik Spoon for supplying the data for the Spoon et al. (2007) diagnostic diagram and the mean IRS spectra for their spectral classes.

## REFERENCES

- Alexander D. M., Efstathiou A., Hough J. H., Aitken D. K., Lutz D., Roche P. F., Sturm E., 1999, MNRAS, 310, 78
- Bruzual A. G., Charlot S., 1993, ApJ, 405, 538
- Clements D. et al., 2008, MNRAS, 387, 247
- Clements D. L., Dunne L., Eales S., 2009, MNRAS, submitted
- Dale D. A., Helou G., Contursi A., Silbermann N. A., Kolhatkar S., 2001, ApJ, 549, 215
- Dopita M. A. et al., 2005, 619, 755
- Dullemond C. P., van Bemmell I. M., 2005, A&A, 436, 47
- Dunne L., Eales S., Edmunds M., Ivison R., Alexander P., Clements D. L., 2000, MNRAS, 315, 115
- Efstathiou A., Rowan-Robinson M., 1990, in Bussolletti E., Vittone A. A., eds, Dusty Objects in the Universe. Kluwer, Dordrecht, p. 197
- Efstathiou A., Rowan-Robinson M., 1995, MNRAS, 273, 649
- Efstathiou A., Rowan-Robinson M., 2003, MNRAS, 343, 322 (ERR03)
- Efstathiou A., Siebenmorgen R., 2005, AA, 439, 85
- Efstathiou A., Siebenmorgen R., 2009, AA, in press
- Efstathiou A., Rowan-Robinson M., Siebenmorgen R., 2000, MNRAS, 313, 734 (ERRS00)
- Farrah D., Afonso J., Efstathiou A., Rowan-Robinson M., Fox M., Clements D., 2003, MNRAS, 343, 585.
- Farrah D. et al., 2008, ApJ, 677, 957
- Fox M., 2002, PhD thesis, Univ. London
- Granato G. L., Danese L., 1994, MNRAS, 268, 235
- Hao L. et al., 2005, ApJ, 625, L75
- Hao L., Weedman D. W., Spoon H. W. W., Marshall J. A., Elitzur M., Houck J. R., 2007, ApJ, 655, L77
- Hernan-Caballero A. et al., 2009, MNRAS, 395, 1695

- Hönig S. F., Beckert T., Ohnaka K., Weigelt G., 2006, *AA*, 452, 459
- Mathis J. S., Mezger P. G., Panagia N., 1983, *AA*, 128, 212
- Nenkova M., Ivezić Z., Elitzur M., 2002, *ApJ*, 570, L9
- Nenkova et al., 2008, *ApJ*, 685, 147
- Pier G. L., Krolik J., 1992, *ApJ*, 401, 99
- Piovan L., Tantalò R., Chiosi C., 2006, *MNRAS*, 366, 923
- Rigopoulou D., Lawrence A., Rowan-Robinson M., 1996, *MNRAS*, 278, 1049
- Roche P. F., Aitken D. K., Smith C. H., Ward M. J., 1991, *MNRAS*, 248, 606
- Rowan-Robinson M., 1992, *MNRAS*, 258, 787
- Rowan-Robinson M., 1995, *MNRAS*, 272, 737
- Rowan-Robinson M., 2001, *ApJ*, 549, 745
- Rowan-Robinson M., 2004, *MNRAS*, 351, 1290
- Rowan-Robinson M., Crawford J., 1989, *MNRAS*, 238, 523
- Rowan-Robinson M., Efstathiou A., 1993, *MNRAS*, 263, 675
- Rowan-Robinson M. et al., 2005, *AJ*, 129, 1183
- Rowan-Robinson M. et al., 2006, in Spitzer Conference ‘Understanding Galaxy Populations’, preprint (astro-ph/0603737)
- Rowan-Robinson M. et al., 2008, *MNRAS*, 386, 697
- Ruiz M., Efstathiou A., Alexander D. M., Hough J., 2001, *MNRAS*, 325, 995
- Schartmann M., Meisenheimer K., Camenzind M., Wolf S., Tristram K. R. W., Henning T., 2008, *A&A*, 482, 67
- Siebenmorgen R., Krügel E., 1992, *A&A*, 259, 614
- Siebenmorgen R., Krügel E., 2007, *AA*, 461, 445
- Siebenmorgen R., Haas M., Krügel E., Schulz B., 2005, *Astron. Nachrichten*, 326, 556
- Silva L., Granato G. L., Bressan A., Danese L., 1998, *ApJ*, 509, 103
- Spoon H. et al., 2007, *ApJ*, 654, L49
- Takagi T., Arimoto N., Hanami H., 2003, *MNRAS*, 340, 813
- Wang L., Rowan-Robinson M., 2009, *MNRAS*, in press

This paper has been typeset from a  $\text{T}_{\text{E}}\text{X}/\text{L}_{\text{A}}\text{T}_{\text{E}}\text{X}$  file prepared by the author.